Evolution in Electrical and Electronic Engineering Vol. 2 No. 2 (2021) 577-587

EEEE

Homepage: http://publisher.uthm.edu.my/periodicals/index.php/eeee
e-ISSN : 2756-8458

Vibration Error Compensation Module for Autonomous Underwater Vehicle (AUV)

Nor Izwana Abd Jalil[1], Herdawatie Abdul Kadir[1]*

[1]Department of Electronic Engineering, Faculty of Electrical and Electronic Engineering,
Universiti Tun Hussein Onn Malaysia, Batu Pahat, 86400, MALAYSIA.

*Corresponding Author Designation

DOI: https://doi.org/10.30880/eeee.2021.02.02.069
Received 16 July 2021; Accepted 01 August 2021; Available online 30 October 2021

Abstract: This project study the Internal Measurement Unit (IMU) vibration error effect for Autonomous Underwater Vehicles (AUV). As the AUV propeller movement speed is induced by a non-uniformity in the flow, it will cause the shaft's propulsion to vibrate. Therefore, to ensure the AUV motion control is more reliable, the shaft vibration must be eliminated from the collected reading. This project reveals the feasible data of position and orientation for navigation, analyses observable errors and tests performance of proposed optimization techniques. The main objectives for this project are to identify the vibration error of the autonomous underwater vehicle (AUV) and integrate the vibration error compensation method for the navigation purpose using MATLAB. Using the filtering technique which is known as Extended Kalman Filter (EKF) IMU reading, the noise of the vibration error will be reduced. The Extended Kalman Filter is used as a system state indicator that uses a preview loop from persistent unregulated assumptions. Furthermore, a projection for the next state is predicted by using data obtained from previous and present states. This prediction is then updated and used based on the observation process, which focuses on estimates and measurements. The end-to-end RMS errors of no disturbance module for x, y and z are 1.17 meters, 0.99 meters and 0.03 meters. Moreover, the end-to-end RMS errors of present disturbance module for x, y and z are 0.57 meters, 0.53 meters and 0.68 meters. These updated estimates may be used with a new statistical calculation. This work will help the AUV to further improve the state estimation and navigation performance.

Keywords: Vibration Error Effect, Autonomous Underwater Vehicles, Extended Kalman Filter

1. Introduction

Autonomous Underwater Vehicles (AUV) are robotic vehicles that can dive, travel or glide in the sea, depending on configuration, without the human controllers having real-time control. Some AUV frequently or continuously communicate with their operators through satellite signals or acoustic

*Corresponding author: watie@uthm.edu.my

lighting underwater to allow these control levels. A wide range of AUV, ranging from tens of kilos weighted vehicles to thousands of kilograms that exist. Since the 1960s, the AUV technical development and occasional experimental use of AUV has been in nature, and repetitive AUV use has been novel for science in recent years [1]. The introduction of AUV led to a growth in investment in the production of AUV technology and in successful industrial AUV and AUV services providers. On the surface, AUV are programmed and then move on their own through the water by gathering information as they go. Compensation for ocean-based research is AUV. Scientists and engineers are generating the necessary operation or behavior of the robot, the cross processes that will develop the functionality or operation, and the specific design concepts. Devices are proposed to model human species, ecosystems, or whole fish populations. Underwater robots may or may not be self-propelled, conductivity autonomous powered by on-board batteries or operated by computers [2]. They can enter shallower water than boats can and deeper water than many tethered vehicles or human divers can.

AUV are capable of measuring water physical characteristics, such as temperature, salinity, dissolved oxygen, detecting microscopic marine algae chlorophyll, measuring water concentrations of small particles, mapping he seafloor, collecting seafloor and mid water photos [3]. AUV are protected from bad weather once deployed and submerged and can remain submerged for extended periods of time. They are also scalable, or modular, meaning that depending on their research goals scientists may choose which sensors to connect to them. Scientists use AUV to study lakes, west coast, and ocean floors. A few devices may be provided to AUV to determine the presence of different aspects or substances, the absorption or reflection of light and the presence of microscopic life [4]. Autonomous underwater vehicles use to investigate air crash investigation such as AUV ABYSS, have been used to find wreckage of missing airplanes Air France Flight 447 and the Bluefin21 AUV was used in the search for Malaysia Airlines Flight 370. The Applied Physics Lab at the University of Washington has been constructing iterations for its Seaglider AUV platform since the1950s. Although iRobot Seaglider was designed for oceanographic research, much interest has taken place from institutions like the U.S. in recent years [5]. The truth of the matter that these autonomous gliders are easy to reproduce and representative of the plurality of AUV systems that will be popular in a variety of applications.

1.1 Introduction of Inertial Measurement Unit (IMU)

An inertial measurement unit (IMU) is an electronic unit that measures, calculates and records acceleration, orientation, angular momentum, and forces of gravity as shown in Figure 1.

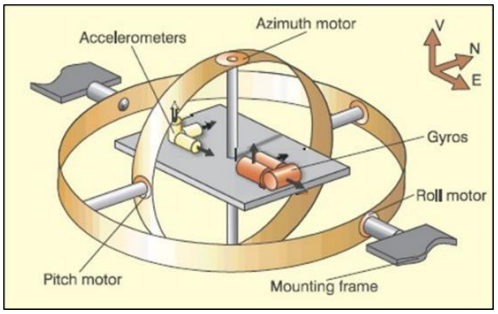

Figure 1: Inertial Measurement Unit (IMU) [6]

IMU usually used at the vehicle or system that have heading reference system such as AUV, UGV, UAV, mobile mapping, gimbal camera and antenna tracking and SAT OTM. IMU consists of three accelerometers, three gyroscopes, and three magnetometers that depending on the heading requirement and there are three vehicle axes which are roll, pitch and yaw. In inertial navigation systems, IMUs also use raw measurements to determine the attitude, angular speeds, linear velocities, and location of the global reference point. The IMU equipped INS is the basis for many commercial and military vehicles including manned aircraft, warheads, ships, submarines, and satellites to be navigated and operated.

The IMU can be installed in GPS-based vehicles or vehicle-tracking devices, allowing the device the ability to count dead and to gather data on the vehicle's current speed, turning velocity, head, inclination, and acceleration as well as the wheel speed sensor output and if available, reverse gear sensor output.

In several consumer goods, in addition to navigational functions IMU also act as orientation sensors. Nearly every smartphone and tablet have IMU as its orientation sensors. Fitness trackers and other wearables can also have activity measuring IMU, for example service. IMU are also able to distinguish innovations of people in motion by defining the specificity and response of running parameters. The data recorded by the IMU are fed to a processor in a navigation system which calculates attitude, speed, and location. A standard application called an inertial strap-down system incorporates angular rate from the gyroscope for angular location measurement. This is coupled in an Extended Kalman Filter to estimate an attitude by the gravities vector determined by the accelerometers. The attitude estimate is used to transform calculations of acceleration into an inertia reference frame, where they are combined once to get a linear velocity and twice to get a linear position. In conjunction with a mechanical document or a digital map database, this guide system could display a pillar where the aircraft is positioned at a certain point on a geographical basis, as in case of a GPS navigation system but not communicated with any external components including satellites or land radio converters, either communicated with or obtained from any external source. This navigation approach is known as dead reckoning.

An IMU is a specific sensor type that occasionally measures the magnet field, angular velocity, and intensity. IMU have 6 axes that consist of 3-axis gyroscope and 3-axis accelerometer. They can also have an extra three-axis magnetometer that is called an IMU 9-axis. In IMU provide 6 DOF (Degree of Freedom) that shown the way of the object able to move. 6 DOF refer to three degree of translation movement and three degrees of rotational movement. The translation movement across *yaw*, *pitch* and *roll* along each axis while degree of rotational movement coordinates at along *x*, *y*, and *z* at each state. The accelerometer is the most common type of movement sensor. It calculates speed along a single axis. Accelerometers calculate in each way linear acceleration and gravity can be measured as a descending force using an accelerometer. Integrating the acceleration shows once a speed estimation and integrating again gives a position estimate. The accelerometer is a not preferred remote estimating tool because of the simultaneous integration. Whereas accelerometers can measure linear acceleration and does not able to measure twist or rotational movement. However, the gyroscopes calculate the angular speed along 3 axes which are pitch (x axis), roll (y axis) and yaw (z axis) as shown in Figure 2.

$$roll, \phi = \tan^{-1} \frac{accelerometer\ y}{accelerometer\ z} \qquad Eq.1$$

$$pitch, \theta = \tan^{-1} \frac{-accelerometer\ x}{\sqrt{Accelerometer\ y^2 + accelerometer\ z^2}} \qquad Eq.2$$

$$yaw, \psi = Compass\ heading \qquad Eq.3$$

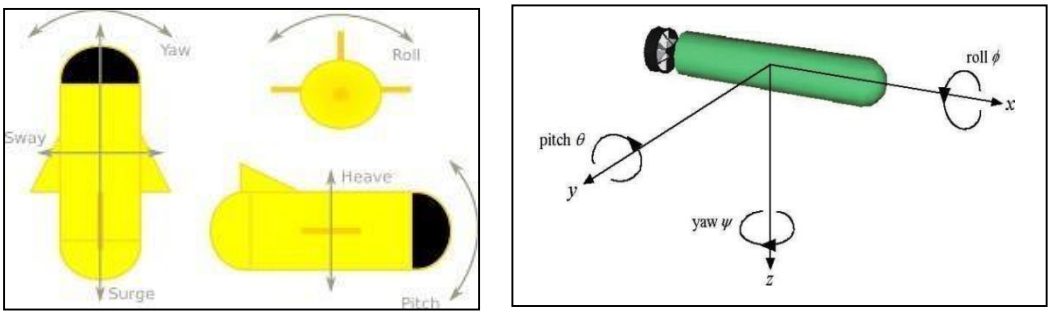

Figure 2: 6 Degree of Freedom (6DoF) of AUV Coordination [7]

2. Methodology

A standard modelling which is AUV using IMU to estimate the vibration error analysis of the vehicle. The modelling will simulate necessary sensor output to measure sensor specifications and performance by specifying sensor performance parameters, such as bias, noise and frequency reaction, among other things. This project will use the MATLAB software to verify the range of the vibration error of the AUV for an IMU sensor device. The sensor will detect the data and the range of the vibration and will be calibrated if error occurs. The project configuration of the mathematical modelling, MATLAB simulation, and sensor detection as shown in Figure 3.

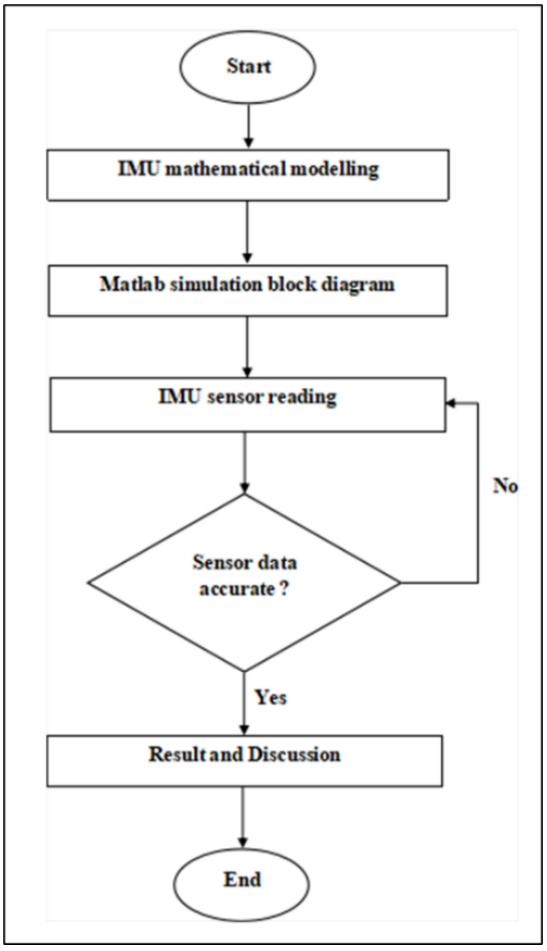

Figure 3: Flowchart of the Project

2.1 Extended Kalman Filter Method

This project will use Extended Kalman Filter (EKF) method to observe the vibration measurement over time. The Extended Kalman Filter is a device that predicts the system status by using a predict-update loop from continuous unverified expectations. In addition, by using data gathered from previous and current state, a forecast for the following state is predicted. This forecast is then revised and used based on the method observation that depends on forecasts and measurements and uncertainties. A new predictive estimate can be made using these revised figures. The state vector will easily describe the Extended Kalman Filter formula phase $Xk-1$ and vector of covariance $Pk-1$ at time $k-1$, when using the following terms $Xk = Fk-1Xk-1 + Vk-1$ where $Fk-1$ physical model represents, and $Vk-1$ will depict Gaussian instability. Then the vector observation is defined as $Zk = HkXk + Wk$ where Hk shows the observation process physical model and Wk will show uncertainty. The two vectors of $Vk-1$ and Wk will depicts the shows of vulnerability. The two vectors of $Vk-1$ and Wk is defined as provided

by zero-medium Gaussian covariance distributions $Qk-1$ and Rk. The Extended Kalman Filter State Vector can be predicted and modified by using the equations.

$Xk|k-1$ and $Pk|k-1$ are the predictive estimates values of the state and covariance vectors, Xk and Pk are the updated estimate values. The Sk is the variety of the $(Zk - HkXk|k-1)$ and Kk the Extended Kalman gain. The revised estimation reveals Xk significant parallels with the forecast $Xk|k-1$ based on the observation differentiation Zk and the forecast observation $HkXk|k-1$. The consequence is the Extended Kalman gain and is high if the variance in prediction is different. The result of this distinction is subject to the Extended Kalman gain and extensive when the difference of the prediction $Pk|k-1$ increases above empirical fluctuations Rk. Consequently, after the observation values are more secure, the predictions will be continuously modified by the Extended Kalman Filter. The Extended Kalman Filter process to measure and observe the vibration measurement as shown in Figure 4.

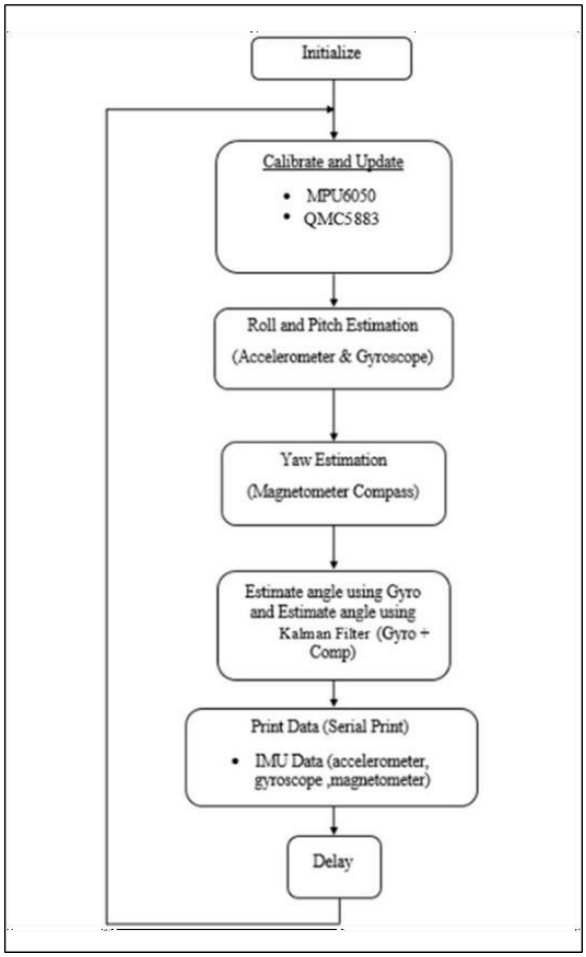

Figure 4: Extended Kalman Filter Processes [8]

3. Results and Discussion

The method model for velocity estimation using IMU sensor data is based on Newton's equation of motion. Newton's universal gravity law is typically said that each particle in the universe attracts all other particles with a force exactly proportional to its mass product and inversely proportional to the square of the distance between its centers. In addition to acceleration, the process model uses angular

rates to distribute the linear velocity based on the following series of equations of x, y, and z as shown in Figure 5.

$$a_x = \dot{U} + (Wq - Vr) + g_x$$
$$a_y = \dot{V} + (Ur - Wp) + g_y$$
$$a_z = \dot{W} + (Vp - Uq) + g_z$$

where (U, V, W) are the velocities along the X-, Y-, and Z-axis, whereas (p, q, r) are the pitch rate, roll rate, and yaw rate, respectively.

Figure 5: The equation of x, y, and z [9]

The flowchart configuration of the simulation in MATLAB as shown in Figure 6. The IMU sensor detect the disturbance and send the measurement to Extended Kalman Filter. Moreover, the Extended Kalman Filter generate and initialize the measurement to set the new reading.

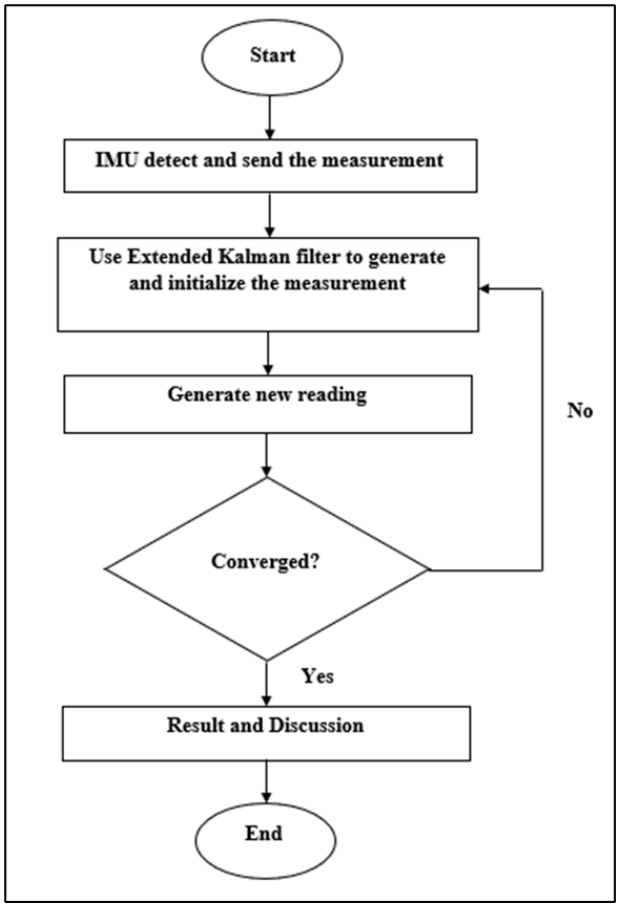

Figure 6: Flowchart of the Simulation

3.1 Result with No Disturbance Module

3.1.1 Position X axis with No Disturbance Module

The graph shows the comparison at the x axis of the estimate position, true position, and position different with no disturbance module error as shown in Figure 7.

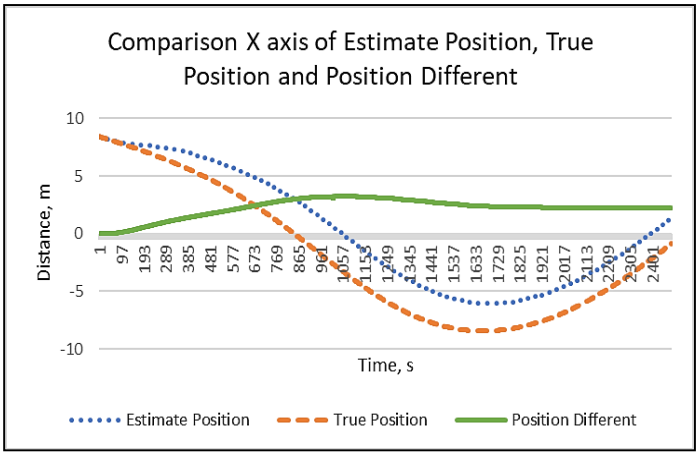

Figure 7: Graph X Axis of The Estimate Position, True Position and Position Different with No Disturbance Module

The graph shows the result of comparison at x axis of the position different between estimate position and true position as shown in Figure 7. The starting point of estimate position and true position are the same. The estimation position and true position differentiate after the starting point, which is the true position and the estimate position have 30% different of the range of the graph. In addition, starting point of the different position located at 0 meter. The result shown the graph flow of the position different is constant and the highest range of the position different was located at 3 meters. It can be concluded that the IMU sensor and GPS fusion had measure the disturbance by using the estimation position and true position to estimate and generate the position different. The end-to-end simulation position RMS error for x position is 2.27 meters.

3.1.2 Position Y axis with No Disturbance Module

The graph shows the comparison at y axis of the estimate position, true position, and position different with no disturbance module as shown in Figure 8.

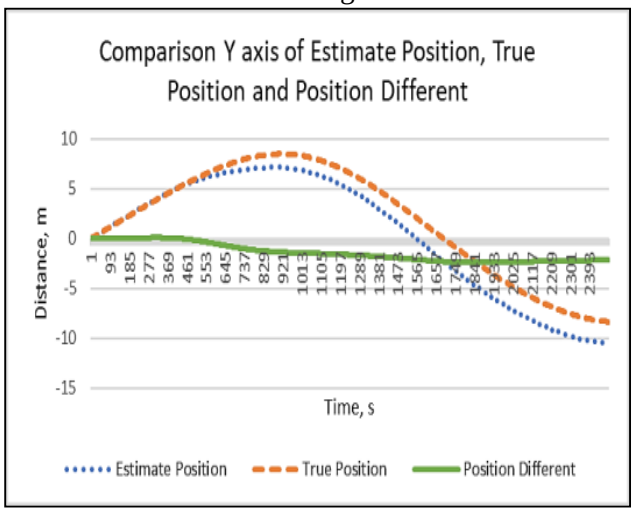

Figure 8: Graph Y Axis of The Estimate Position, True Position and Position Different with No Disturbance Module

The graph displays the difference between the estimated position and true position at x axis as illustrated in Figure 8. Starting point of the estimate position, true position, and position different are corresponding which are 0 meter. Moreover, the estimate position and true position enlargement afterwards starting point. The non-identical of estimate position and true position are fairly which are just 10% different. Position different of the y axis is continuous and the range has slighter fall off when

the peak of the estimation position and true position had increased. The consequence of the graph is there having a slighter different starting from 645 seconds which means 10.75 minutes between estimate position and true position. This differentiate has configure the position different that has constant value. The end-to-end simulation position RMS error for y position is 1.72 meters.

3.1.3 Position Z axis with No Disturbance Module

The graph shows the comparison at z axis of the estimate position, true position, and position different with no disturbance module as shown in Figure 9.

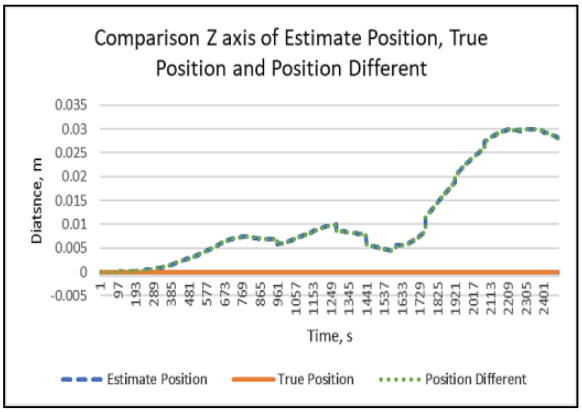

Figure 9: Graph Z Axis of The Estimate Position, True Position and Position Different with No Disturbance Module

The graph illustrates the comparison at the z axis between the estimate position and the actual position as shown in Figure 9**.** Initial point for the estimate position, true position, and position different are at the corresponding point which are 0 meter. The patterns of the estimate position and position different are comparable. In addition, there is no difference in estimate and different position. There is no point other than estimate point in position different assume as the pattern is fixed and the difference position may correspond with an estimated position because the real position has maintained zero. The end-to-end simulation position RMS error for z position is 0.01 meters.

3.2 Result with Present Disturbance Module

3.2.1 Position X axis with Present Disturbance Module

The graph shows the comparison at x axis of the pq position, trajectory position and position different with disturbance module shown Figure 10.

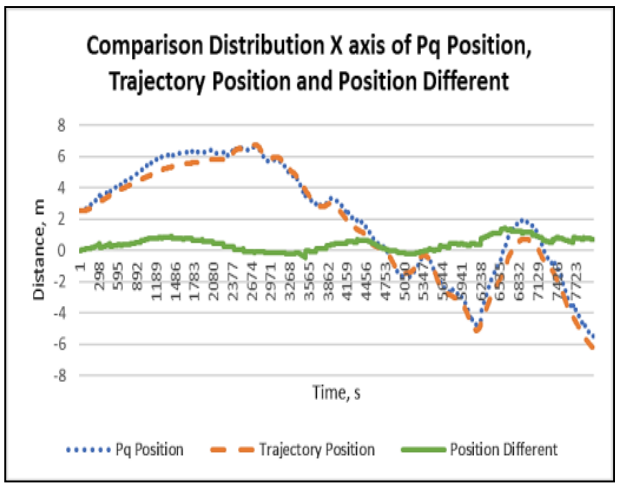

Figure 10: Graph X Axis of the Pq Position, Trajectory Position and Position Different with Disturbance Module

The graph demonstrates a disturbance module as indicated in Figure 3.6 for the comparison of pq position, trajectory position, and position different at x axis. The initial point of the pq position and trajectory position are 100% equivalent. Moreover, the similarity range of the pq position and trajectory position have insignificantly different at 1189 until 2080 seconds which means 19 minutes until 34 minutes. The graph shown the position different against pq position and trajectory position are uniform. In addition, these phenomena had been concluded that the constant range of the position different due to the correction that had been done by the disturbance module between the pq position and trajectory position. The end-to-end simulation position RMS error for x position is 0.57 meters.

3.2.2 Position Y axis with Present Disturbance Module

The graph shows the comparison at y axis of the pq position, trajectory position and position different with disturbance module as shown in Figure 11.

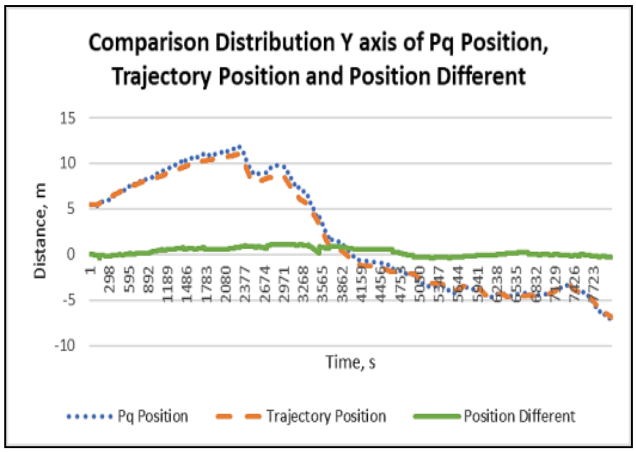

Figure 11: Graph Y Axis of the Pq Position, Trajectory Position and Position Different with Disturbance Module

The graphic displays a disturbance module that compares the pq position, trajectory position and position different of z axis as illustrated in Figure 11. The point of origin for pq position and trajectory position are equivalent. Moreover, the pq position similarity range was accomplished at 2971 seconds that equals 49 minutes. The result of the comparison demonstrates the position different against pq position and trajectory position are sustained due to cumulation of the error. Furthermore, these occurrences were determined that there is no distinct position between pq position and trajectory position, due to the continuous range of both positions. The end-to-end simulation position RMS error for y position is 0.53 meters.

3.2.3 Position Z axis with Present Disturbance Module

The graph shows the comparison at z axis of the pq position, trajectory position and position different with a disturbance module as shown in Figure 12.

The graph illustrates a disturbance module comparing the pq position, trajectory position and position different of the z axis as shown in Figure 12. The initial point of the graphs is almost slightly in same range which means 0-2 meters for pq position and trajectory position and position different. The same pattern of the pq position with trajectory position have an insignificant different at 6238 until 7723 seconds equal to 103 until 128 minutes. Pq position against trajectory position had been measured the consistent range for the position different due to the cumulation of the environmental noise. The end-to-end simulation position RMS error for z position is 0.68 meters.

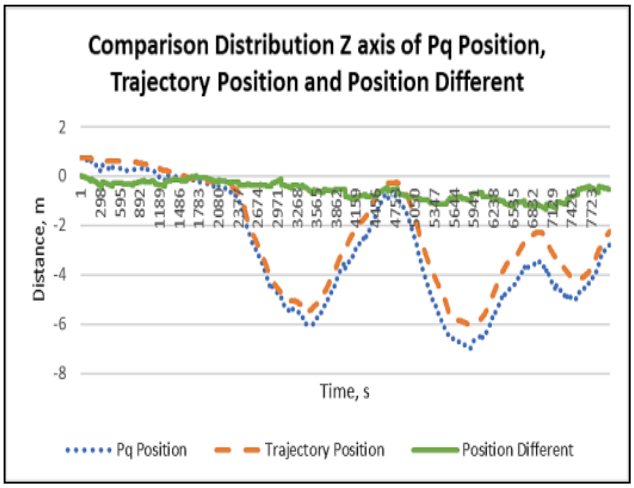

Figure 12: Graph Z Axis of the Pq Position, Trajectory Position and Position Different with Disturbance Module

4. Conclusion

In this final year project had been tested the AUV and Navigation System Principles by using the MATLAB software. The AUV modelling utilize the IMU by estimate the analysis of the underwater vehicle vibration inaccuracy. Furthermore, the system had examined the present of the environmental noise by using the outlier detection that would ensure there is no distribution and inaccuracy between ground truth and estimated position. Hence, the graph pattern of the position different among the phenomenon with the present of the environmental noise and without environmental noise which means no distribution had been illustrated and configured by using the parameters form the MATLAB software. The result of the experimental without distribution module shown that position different at axis x,y and z are mostly have a constant pattern. Moreover, there are minimal error of the position different at axis x,y and z for the graph that had present the disturbance module due to the continuous range of the patterns. From the overall point of view, it can be concluded that the vibration error compensation module for autonomous underwater vehicle had achieved the objectives of the system The underwater navigation has to implement the operation of the IMU and the GPS fusion to assistance the vibration module or any disturbance problems efficiently.

Acknowledgement

The authors would like to thank the Faculty of Electrical and Electronic Engineering, Universiti Tun Hussein Onn Malaysia for its support.

References

[1] J. G. Bellingham, "Learn more about Autonomous Underwater Vehi- cle Platforms: Autonomous Underwater Vehicles Vertical Profiling of Currents Using Acoustic Doppler Current Profilers," *ScienceDirect*, vol. 12, 2009

[2] J. González-García, A. Gómez-Espinosa, E. Cuan-Urquizo, L. G. García-Valdovinos, T. Salgado-Jiménez, and J. A. Escobedo Cabello, "Autonomous underwater vehicles: Localization, navigation, and communication for collaborative missions," *Appl. Sci.*, vol. 10, no. 4, 2020

[3] S. Liu, H. Xu, Y. Lin, and L. Gao, "Visual navigation for recovering an AUV by another AUV in shallow water," *Sensors (Switzerland)*, vol. 19, no. 8, pp. 1–19, 2019

[4] M. She and L. Tian, "A novel path control algorithm for networked underwater robot," *J. Robot.*, vol. 2018, 2018

[5] P. Linke and K. Lackschewitz, "Autonomous Underwater Vehicle „ABYSS"," *J. large-scale Res. Facil. JLSRF*, vol. 2, pp. 1–5, 2016

[6] S. A. Quadri and O. Sidek, "Error and Noise Analysis in an IMU using Kalman Filter Error and Noise Analysis in an IMU using Kalman Filter," no. June, 2014

[7] O. Elijah *et al.*, "A concept paper on smart river monitoring system for sustainability in river," *Int. J. Integr. Eng.*, vol. 10, no. 7, pp. 130–139, 2018

[8] D. Kim, "Application of Kalman Filter for Estimating a Process Disturbance in a Building Space," no. 1, 2017

[9] J. K. Shiau and I. C. Wang, "Unscented Kalman filtering for attitude determination using MEMS sensors," *J. Appl. Sci. Eng.*, vol. 16, no. 2, pp. 165–176, 2013